

# A Monte Carlo examination for the numerical values of universal quantities in spatial dimension two

Fu-Jiun Jiang\*

*Department of Physics, National Taiwan Normal University,  
88, Sec.4, Ting-Chou Rd., Taipei 116, Taiwan*

*\*Corresponding author. Email: fjjiang@ntnu.edu.tw*

By simulating a two-dimensional (2D) dimerized spin-1/2 antiferromagnet with the quantum Monte Carlo method, the numerical values of two universal quantities associated with the quantum critical regime (QCR), namely  $S(\pi, \pi)/(\chi_s T)$  and  $c/(T\xi)$ , are determined. Here  $S(\pi, \pi)$ ,  $\chi_s$ ,  $c$ ,  $\xi$ , and  $T$  are the staggered structure factor, the staggered susceptibility, the spin-wave velocity, the correlation length, and the temperature, respectively. For other QCR universal quantities, such as the Wilson ratio  $W$  and  $\chi_u c^2/T$  ( $\chi_u$  is the uniform susceptibility), it is shown that the addition of higher order theoretical contribution makes the agreement between the numerical and the analytic results worse. We find that the same scenario applies to  $S(\pi, \pi)/(\chi_s T)$  and  $c/(T\xi)$  as well. Specifically, our calculations lead to  $S(\pi, \pi)/(\chi_s T) \sim 1.073$  and  $c/(T\xi) \sim 0.963$  which are in better consistence with the leading theoretical predictions than those with the next-to-leading order terms. The presented outcome here as well as those in some relevant literature suggest that it is desirable to conduct a refinement of the analytic calculation to resolve the puzzle of why the inclusion of higher order terms leads to less accurate predictions for these universal quantities.

## I. INTRODUCTION

For systems in spatial dimension two which have short-range interactions, the associated continuous symmetry cannot be broken spontaneously (at finite temperature  $T$ ) due to the famous Mermin–Wagner theorem [1]. Therefore, for these systems, instead of a (finite-temperature) phase transition, an exotic region called quantum critical regime (QCR) emerges.

Physical quantities related to QCR have been analytically calculated in detail in Refs. [2–4]. These quantities are universal, namely their values only depend on the macroscopic, not the microscopic features of the considered system(s). For two-dimensional (2D) quantum spin antiferromagnetic models, these universal quantities include the Wilson ratio  $W$ ,  $\chi_u c^2/T$ ,  $S(\pi, \pi)/(\chi_s T)$ , and  $c/(\xi T)$ . Here,  $\chi_u$ ,  $c$ ,  $S(\pi, \pi)$ ,  $\chi_s$ , and  $\xi$  are the uniform susceptibility, the spin-wave velocity, the staggered structure factor, the staggered susceptibility, and the correlation length, respectively.

In Ref. [4], based on the effective  $O(N)$  nonlinear sigma model, the numerical values for the universal quantities mentioned in the previous paragraph have been determined to next-to-leading order in the large  $N$ -expansion. The analytic calculations lead to  $W \sim 0.1147$ ,  $\chi_u c^2/T \sim 0.27185$ ,  $S(\pi, \pi)/(\chi_s T) \sim 1.09$ , and  $c/(\xi T) \sim 1.04$ .

Some of these quantities have been investigated using the first principle non-perturbative quantum Monte Carlo simulations (QMC) in several studies [4–13]. Although earlier calculations of Ref. [4, 5, 8, 9] conclude that the Monte Carlo results agree well with the theoretical predictions, later computations in Ref. [10–13] observe non-negligible deviations between the QMC results and the analytic predictions. In particular, it is found in Ref. [10–13] that  $W \sim 0.1248(0.1238)$  and  $\chi_u c^2/T \sim 0.32(0.33)$ . Both the values of  $W$  and  $\chi_u c^2/T$ , determined by the exact method, namely the QMC, differ from the associated analytic predictions by at least around 10 percent.

Interestingly, as pointed out in Ref. [10], with only the leading contributions, the agreement between the analytic and the numerical outcomes for  $W$  and  $\chi_u c^2/T$  is remarkably good. Table 1 lists the theoretical leading results, up to the order  $1/N$  outcomes as well as the Monte Carlo determinations for  $W$  and  $\chi_u c^2/T$ . As can be seen from the table, the leading terms match the numerical results well, and the addition of order  $1/N$  corrections makes the agreement between the theoretical and the numerical values for  $W$  and  $\chi_u c^2/T$  worse. It will be interesting to examine whether this scenario is systematic by computing other universal quantities of QCR through an exact approach.

In this study, we perform large-scale Monte Carlo simulations to determine the numerical values of  $S(\pi, \pi)/(\chi_s T)$  and  $c/(T\xi)$  of a 2D dimerized quantum antiferromagnetic Heisenberg model. Dimerized quantum antiferromagnets and their spatially isotropic versions have been employed for many investigations regarding examining certain theoretical predictions, such as the universality class of quantum phase transitions as well as the values of the low-energy constants from the related effective field theories [14–23].

By extrapolating the data on linear system size  $L = 512$  with various temperatures, we arrive at  $S(\pi, \pi)/(\chi_s T) \sim 1.073$ . Similar calculation leads to  $c/(T\xi) \sim 0.963$ . Remarkably, like  $W$  and  $\chi_u c^2/T$ , the theoretical leading contributions for  $S(\pi, \pi)/(\chi_s T)$  and  $c/(T\xi)$  agree with our results well, see table 1. The outcomes demonstrated in table 1 suggest strongly that theoretical leading terms have better agreement with the numerical values of the universal

Universal quantity	Leading order	Up to next-to-leading order	Monte Carlo
$W$	0.1243	0.1147	0.1248(3) (0.1238(3))
$\chi_u c^2/T$	0.3425	0.27185	0.33(1)
$S(\pi, \pi)/(\chi_s T)$	1.076	1.09	1.0727(2)
$c/(T\xi)$	0.962424	1.0386	0.963(6)

TABLE I: The theoretical and Monte Carlo results for the numerical values of  $W$ ,  $\chi_u c^2/T$ ,  $S(\pi, \pi)/(\chi_s T)$ , and  $c/(T\xi)$  (These values are from Refs. [4, 10–13] and present work).

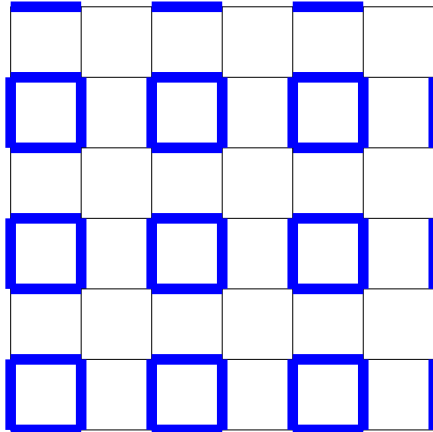


FIG. 1: The plaquette model considered in this study. The thick and thin bonds represent the couplings of strength  $J_2$  and  $J_1$ , respectively. The figure is from Ref. [11].

quantities of QCR than those including the  $1/N$  corrections is a systematic trend.

It should be pointed out that the quantity  $S(\pi, \pi)/(\chi_s T)$  associated with the considered 2D dimerized quantum Heisenberg model has been studied in Ref. [11]. Here we simulate larger lattices and lower temperatures so that the bulk result can be obtained with the systematic errors being (nearly) eliminated in principle. The  $c/(T\xi)$  data shown here were obtained sometime ago [11], but are never published.

The presented outcomes in this study as well as those in Ref. [10–13] suggest that it will be desirable to refine the associated analytic calculations to resolve the puzzle of why the addition of high order corrections leads to worse agreement between the numerical and the theoretical values for these universal quantities.

The rest of the paper is organized as follows. After the introduction, the model and the measured observables are described in Sec. II. We then present the obtained results in Sec. III. Sec. VI contains the conclusions of the present study.

## II. THE CONSIDERED MODEL AND OBSERVABLES

The Hamiltonian of the studied 2D quantum dimerized plaquette Heisenberg model has the form

$$H = \sum_{\langle ij \rangle} J_1 \vec{S}_i \cdot \vec{S}_j + \sum_{\langle i' j' \rangle} J_2 \vec{S}_{i'} \cdot \vec{S}_{j'}, \quad (1)$$

where  $J_1$  and  $J_2$  are the antiferromagnetic couplings connecting nearest neighbor spins  $\langle ij \rangle$  and  $\langle i' j' \rangle$ , respectively, and  $\vec{S}_i$  is the spin- $\frac{1}{2}$  operator at site  $i$ . Fig. 1 shows the graphical representation of the considered model. In this study, we let  $J_1$  be 1 and vary the value of  $J_2$  so that a phase transition from the ordered phase to the disordered order takes place at a particular value of  $J_2 > J_1$ . It is known in the literature that the value of  $J_2/J_1$  where the mentioned phase transition occurs is  $J_2/J_1 = 1.8230(2)$  [24] (This particular value is typically denoted by  $(J_2/J_1)_c$  in the literature).

To obtain a high precision value for the universal quantity  $S(\pi, \pi)/(\chi_s T)$  and  $c/(T\xi)$  of QCR, the staggered structure factor  $S(\pi, \pi)$ , the staggered susceptibility  $\chi_s$ , the correlation length  $\xi$ , and spin-wave velocity  $c$  are calculations

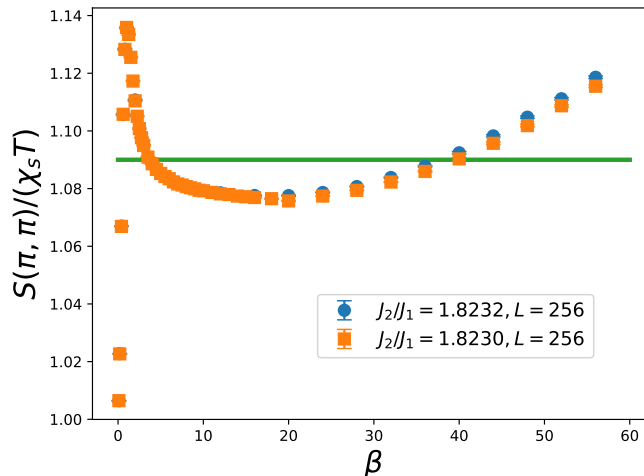


FIG. 2:  $S(\pi, \pi)/(\chi_s T)$  as functions of  $\beta$  for  $J_2/J_1 = 1.8230$  and  $1.8232$ . Part of the data are from Ref. [11].

from the QMC. On a (squared) system with linear size  $L$  and inverse temperature  $\beta$ ,  $S(\pi, \pi)$  and  $\chi_s$  are defined as

$$S(\pi, \pi) = 3L^2 \langle (m_s^z)^2 \rangle \quad (2)$$

$$\chi_s = 3L^2 \int_0^\beta \langle m_s^z(\tau) m_s^z(0) \rangle d\tau, \quad (3)$$

where  $m_s^z = \frac{1}{L^2} \sum_i^N (-1)^{i+i_2} S_i^z$  with  $N = L^2$ . In addition,  $\xi$  is given by  $\xi = 0.5(\xi_1 + \xi_2)$ , where  $\xi_1$  and  $\xi_2$  are defined as

$$\begin{aligned} \xi_1 &= \frac{L}{2\pi} \sqrt{\frac{S(\pi, \pi)}{S(\pi + 2\pi/L, \pi)} - 1} \\ \xi_2 &= \frac{L}{2\pi} \sqrt{\frac{S(\pi, \pi)}{S(\pi, \pi + 2\pi/L)} - 1}, \end{aligned} \quad (4)$$

here the quantities  $S(\pi + 2\pi/L, \pi)$  and  $S(\pi, \pi + 2\pi/L)$  are the Fourier modes with the second largest magnitude. Finally, the spin-wave velocity  $c$  is obtained through the temporal and spatial winding numbers squared ( $\langle W_i^2 \rangle$  and  $\langle W_i^2 \rangle$  with  $i \in \{1, 2\}$ ).

### III. NUMERICAL RESULTS

To calculate the numerical values of  $S(\pi, \pi)/(\chi_s T)$  and  $c/(T\xi)$  in an exact approach, we have performed large-scale quantum Monte Carlo calculations (QMC) using the stochastic series expansion algorithm (SSE) with efficient operate-loop update [25]. The outcomes obtained are detailed below.

#### 1. $S(\pi, \pi)/(\chi_s T)$

It is known that the critical point  $(J_2/J_1)_c$  for the chosen dimerized quantum antiferromagnetic model is given by  $1.8230(2)$  [24]. Therefore, for  $L = 256$  we have carried out calculations with  $J_2/J_1 = 1.8230$  and  $1.8232$ . The resulting  $S(\pi, \pi)/(\chi_s T)$  as functions of  $\beta$  are shown in fig. 2. As can be seen in the figure, the deviation of the values for  $S(\pi, \pi)/(\chi_s T)$  due to the variant of  $(J_2/J_1)_c$  within the error bar is very mild. As a result, we have conducted the investigation at  $J_2/J_1 = 1.8230$ .

Figure 3 shows  $S(\pi, \pi)/(\chi_s T)$  as functions of  $\beta$  for  $L = 128$  and  $L = 256$ . The results in the figure imply that the finite-size effect starts to become serious when the data curve associated with the smaller  $L$  begins to rise with  $\beta$ . A similar trend is also observed for the data associated with  $L = 256$  and  $L = 512$ , see fig. 4.

Based on the observation described above and shown in figs. 3 and 4, it is beyond doubt that the deviation of  $L = 512$  data from the corresponding bulk ones is insignificant since the trend of  $L = 512$  data still moves downward

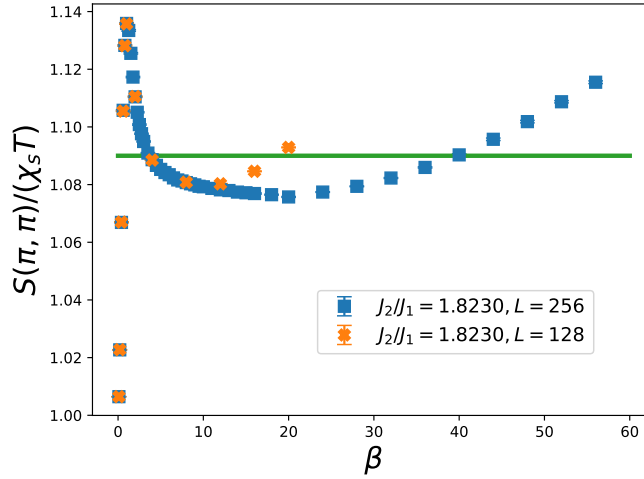


FIG. 3:  $S(\pi, \pi)/(\chi_s T)$  as functions of  $\beta$  at  $J_2/J_1 = 1.8230$  for  $L = 128$  and  $L = 256$ . Part of the data are from Ref. [11].

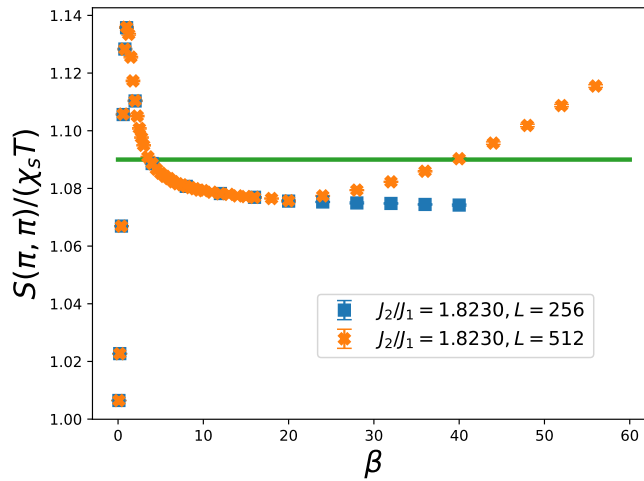


FIG. 4:  $S(\pi, \pi)/(\chi_s T)$  as functions of  $\beta$  at  $J_2/J_1 = 1.8230$  for  $L = 256$  and  $L = 512$ . Part of the data are from Ref. [11].

for the used values of  $\beta$ . By applying the ansatz  $a + b/\beta$  to fit the  $L = 512$  data with  $\beta > 4.0$  leads to  $a = 1.0727(2)$ . With this fitting result one arrives at  $S(\pi, \pi)/(\chi_s T) \sim 1.0727(2) \sim 1.073$ . Figure 5 demonstrates the  $L = 512$  data of  $S(\pi, \pi)/(\chi_s T)$  as a function of  $\beta$ . The solid curve appearing in the figure is obtained by using the fitting results. Finally, the horizontal solid and dashed lines are 1.09 and 1.0727, respectively.

## 2. $c/\{(T\xi)$

The calculation of  $c/(T\xi)$  requires the numerical value of  $c$ . The quantity  $c$  can be determined by the temporal and spatial winding numbers squared  $\langle W_t^2 \rangle$  and  $\langle W^2 \rangle = 0.5 (\langle W_1^2 \rangle + \langle W_2^2 \rangle)$  [26]. Specifically, for a given  $L$ , one varies  $\beta$  so that  $\langle W_t^2 \rangle$  and  $\langle W^2 \rangle$  take about the same values. When this condition is met, the  $c(L)$  associated with the given  $L$  is  $c(L) = L/\beta$ . With the obtained  $c(L)$  on several finite lattices, one can determine the bulk  $c$  by extrapolating the data of  $c(L)$ .

The spin-wave velocity required for determining  $c/\{(T\xi)$  has been calculated in Ref. [11] and has a value of 2.163(4).  $c/(T\xi)$  as a function of  $\beta$  is depicted in fig. 6. For each value of  $\beta$ , the associated  $c/(T\xi)$  is either the bulk one or has nearly negligible finite-size effect. Therefore, conducting fits using the data shown in the figure should lead to reliable zero temperature result for  $c/(T\xi)$ . With fits by employing the ansatz  $a + b/\beta$ , we arrive at  $a = 0.963(6)$  which is the zero temperature value for  $c/(T\xi)$ . The obtained  $c/(T\xi) = 0.963(6)$  agrees reasonably well with the leading order analytic prediction 0.962424, but deviates from the result of adding next-to-leading order contribution 1.04.

Fig. 7 shows the  $L$ -dependence of  $c/(T\xi)$  for two values of inverse temperature  $\beta = 8.0$  and  $\beta = 10.0$ . As can be seen from the figure, the magnitude of  $c/(T\xi)$  decreases as  $\beta$  increases. Hence, if the the data shown in fig. 6 are

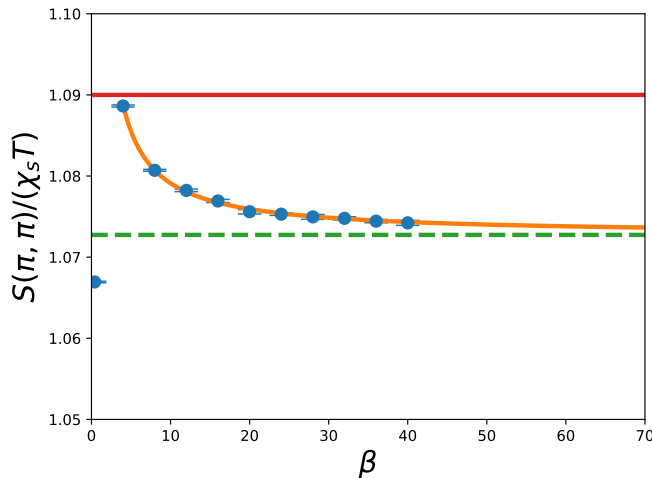


FIG. 5:  $S(\pi, \pi)/(\chi_s T)$  as a function of  $\beta$  at  $J_2/J_1 = 1.8230$  for  $L = 512$ . The solid curve is obtained by using the results of the fits. The horizontal solid and dashed lines represent 1.09 (up to next to leading order prediction) and 1.0727 (leading order prediction), respectively.

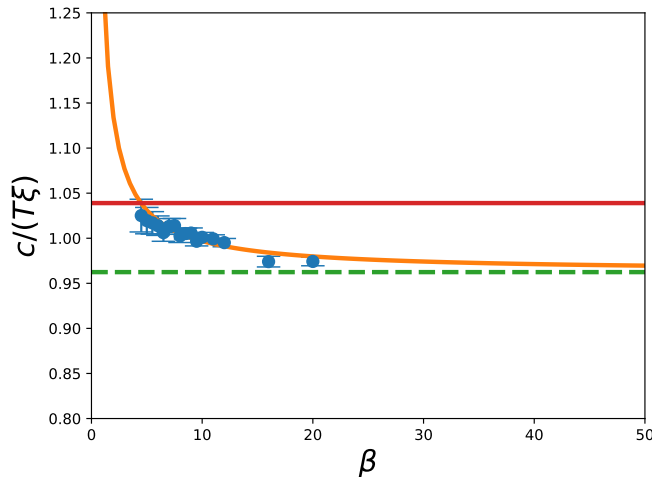


FIG. 6:  $c/(T\xi)$  as a function of  $\beta$  at  $J_2/J_1 = 1.8230$ . The solid curve is obtained by using the results of the fits. The horizontal solid and dashed lines represent 1.04 (up to next to leading order prediction) and 0.962424 (leading order prediction), respectively.

slightly away from their bulk ones, then one expects that the bulk data curve will lower a little bit. This scenario will lead to the same conclusion as claimed in the previous paragraph. Specifically, the leading analytic prediction matches better with the numerical result than the one including the next-to-leading order contribution.

### 3. $\chi_u c^2/T$ and $W$

For completeness, we reproduce the results associated with  $\chi_u c^2/T$  and  $W$  using the data of Refs. [13] and [12]. These data are obtained by simulating the 2D dimerized Herringbone quantum Heisenberg model.

The left panel of fig. 8 is the quantity  $\chi_u c^2/T$  as functions of the inverse temperature  $\beta$  calculated in Ref. [13]. The dashed and solid lines in the figure are the leading order and up to next-to-leading order theoretical predictions. It is clear from the figure that the leading order result has better match with the numerical data than that including the next-to-leading order contribution.

Finally, the right panel of fig. 8 is the Wilson ratio  $W$  obtained in Ref. [12] ( $W = 0.1238(3)$ ). Similar to the left panel of fig. 8, the dashed and solid lines in the figure represent the leading order and up to next-to-leading order analytic outcomes. It is beyond doubt from the figure that the agreement between the numerical data and the leading order result is much better than that when one compares the data with the prediction including the next-to-leading order contribution.

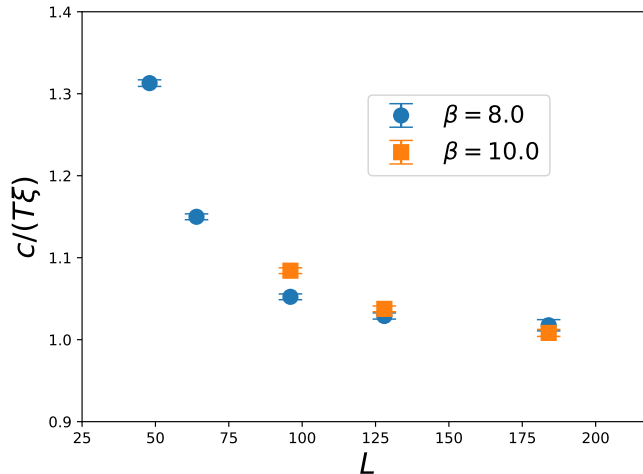


FIG. 7:  $c/(T\xi)$  as a function of  $L$  at  $J_2/J_1 = 1.8230$  for two values of inverse temperature  $\beta = 8.0$  and  $\beta = 10.0$ .

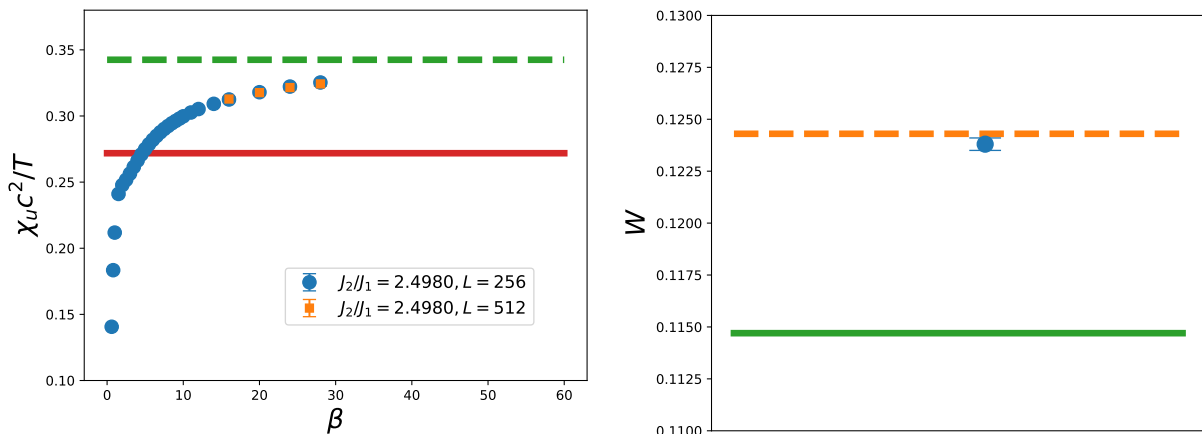


FIG. 8: (Left)  $\chi_u c^2/T$  as functions of the inverse temperature  $\beta$  [13]. (Right) The value of Wilson ratio  $W$  ( $W = 0.1238(3)$ ) [12]. In both panels, the dashed and solid lines represent the leading order and up to next-to-leading order theoretical predictions, respectively.

#### IV. DISCUSSIONS AND CONCLUSIONS

In this study, we simulate the 2D dimerized quantum plaquette Heisenberg model using QMC. In addition, fitting the relevant data obtained on large lattices and at moderate low temperatures, we find that the numerical values of  $S(\pi, \pi)/(\chi_s T)$  and  $c/(T\xi)$  are given by  $S(\pi, \pi)/(\chi_s T) \sim 1.073$  and  $c/(T\xi) \sim 0.963$ .

Based on the presented outcomes here and those in Refs. [10, 12, 13], it is unexpected that for these four quantities  $W$ ,  $\chi_u c^2/T$ ,  $S(\pi, \pi)/(\chi_s T)$ , and  $c/(T\xi)$  of QCR, the leading large- $N$  expansion calculations lead to better agreement between the theoretical and the numerical values than the ones including the  $1/N$  corrections. It will be extremely interesting to understand whether this trend can be explained rigorously from an analytic point of view. Finally, since in all these cases, the  $N$  in the large  $N$ -expansion calculations is 3 which is not large, it is also likely that a calculation to the next-to-next-to-leading order may coincide the results of Monte Carlo with those of analytic computations.

In conclusion, it is desirable to conduct further theoretical calculations to resolve the puzzle of the numerical and the theoretical results for these universal quantities shown in this study and in Refs [10, 12, 13].

#### Acknowledgement

We thank D.-R. Tan and J.-H. Peng for their involvement in Refs. [11] and [12].

## Funding

Partial support from National Science and Technology Council (NSTC) of Taiwan is acknowledged (Grant numbers: NSTC 112-2112-M-003-016- and NSTC 113-2112-M-003-014-).

## Conflict of Interest

The author declares no conflict of interest.

## Data Availability Statement

Data are available from the corresponding author on reasonable request.

- 
- [1] N. D. Mermin and H. Wagner, Phys. Rev. Lett. **17**, (1966) 1133.
  - [2] A. V. Chubukov and S. Sachdev, Phys. Rev. Lett. **71**, 169 (1993).
  - [3] A. V. Chubukov and S. Sachdev, Phys. Rev. Lett. **71**, 2680 (1993).
  - [4] A. V. Chubukov, S. Sachdev, and J. Ye, Phys. Rev. B **49**, (1994) 11919.
  - [5] A. W. Sandvik, A. V. Chubukov, and S. Sachdev, Phys. Rev. B **51**, 16483 (1995)
  - [6] M. Troyer, H. Kantani, and K. Ueda, Phys. Rev. Lett. **76**, 3822 (1996).
  - [7] Matthias Troyer, Masatoshi Imada, and Kazuo Ueda, J. Phys. Soc. Jpn. **66**, 2957 (1997).
  - [8] Jae-Kwon Kim and Matthias Troyer, Phys. Rev. Lett. **80**, (1998) 2705.
  - [9] Y. J. Kim and R. J. Birgeneau, Phys. Rev. B **62**, 6378 (2000).
  - [10] A. Sen, H. Suwa, and A. W. Sandvik, Phys. Rev. B **92**, (2015) 195145.
  - [11] D.-R. Tan and F.-J. Jiang, Phys. Rev. B **98**, (2018) 245111.
  - [12] J.-H. Peng, D.-R. Tan, and F.-J. Jiang, Phys. Rev. B **102**, 214206 (2020).
  - [13] Fu-Jiun Jiang, Results in Physics **44** (2023) 106119.
  - [14] A. W. Sandvik and M. Vekic, Phys. Rev. Lett. **74**, 1226 (1995).
  - [15] B. B. Beard and U.-J. Wiese, Phys. Rev. Lett. **77**, 5130 (1996).
  - [16] A. W. Sandvik, Phys. Rev. B **56**, 11678 (1997).
  - [17] K. H. Höglund and A. W. Sandvik, Phys. Rev. Lett. **91**, 077204 (2003).
  - [18] S. Wenzel, L. Bogacz, and W. Janke, Phys. Rev. Lett. **101**, 127202 (2008).
  - [19] F.-J. Jiang, F. Kämpfer, and M. Nyfeler, Phys. Rev. B **80**, 033104 (2009).
  - [20] S. Jin and A. W. Sandvik, Phys. Rev. B **85**, 020409(R) (2012).
  - [21] F.-J. Jiang, Phys. Rev. B **85** 014414 (2012).
  - [22] Shinya Yasuda and Synge Todo, Phys. Rev. E **88** 061301 (2013).
  - [23] D.-R. Tan and F.-J. Jiang, Phys. Rev. B **95**, 054435 (2017).
  - [24] S. Wenzel and W. Janke, Phys. Rev. B **79**, 014410 (2009).
  - [25] A. W. Sandvik, Phys. Rev. B **55**, (1999) R14157.
  - [26] F.-J. Jiang, Phys. Rev. B **83**, (2011) 024419.